processes

MDPI

Article

A Dissolution Kinetic Study of Disperse Dye in Supercritical Carbon Dioxide to Design an Efficient Supercritical Dyeing Process

Geonhwan Park, Dong Eui Kwon, Wonbae Kong, Jimin Park and Youn-Woo Lee *

School of Chemical and Biological Engineering & Institute of Chemical Processes, Seoul National University, 1 Gwanak-ro, Gwanak-gu, Seoul 08826, Korea; yooga@snu.ac.kr (G.P.); sot5656@snu.ac.kr (D.E.K.); gore2001@snu.ac.kr (W.K.); tokobomul@snu.ac.kr (J.P.)
* Correspondence: ywlee@snu.ac.kr

Abstract: The dissolution behavior of dye in supercritical carbon dioxide influences the overall mass transfer that controls a supercritical dyeing process. Increasing the dissolution rate of the dye leads to shortening of the dyeing process time and can improve the efficiency of the process. Controlling the properties of the carbon dioxide flow is a good method to improve the dissolution rate of dyes. In this study, a dissolution kinetic model was designed by quantitatively analyzing and formulating the dissolution phenomenon of dyes using an in situ UV/Vis spectrometer. Through this model, the dissolution rate was compared by varying the geometric shape of the column containing the dye and the flow rate of carbon dioxide. Moreover, the correlation equation between the Reynolds number and Sherwood number was obtained through mass transfer coefficients derived under various conditions. In order to verify the utility of this equation, it was applied to a scaled-up device and the precise result could be predicted. This study can be useful in the design of dyeing processes and make-up equipment.

Keywords: supercritical dyeing; dissolution rate; mass transfer coefficient; dimensionless correlation; L/D ratio

check for updates

Citation: Park, G.; Kwon, D.E.; Kong, W.; Park, J.; Lee, Y.-W. A Dissolution Kinetic Study of Disperse Dye in Supercritical Carbon Dioxide to Design an Efficient Supercritical Dyeing Process. *Processes* **2021**, *9*, 977. https://doi.org/10.3390/pr9060977

Academic Editor: Gurutze Arzamendi

Received: 10 May 2021
Accepted: 29 May 2021
Published: 31 May 2021

1. Introduction

Supercritical dyeing has been considered as a viable alternative to water-based dyeing, which leads to environmental pollution. This is because supercritical dyeing employs supercritical carbon dioxide as a dyeing solvent instead of water, avoiding the generation of wastewater that causes environmental pollution, and the use of other chemical substances, such as dispersants and surfactants. It is also energy-efficient, as no additional drying process is required [1,2]. However, there remain efficiency limitations in areas such as process capacity, processing time, and fiber diversity. Many studies have been conducted to improve the supercritical dyeing process [3–5]. Supercritical dyeing is known to consist of the following processes: (1) Dissolution of the dye in supercritical carbon dioxide, (2) transfer of the supercritical carbon dioxide solution to a fiber interface, (3) adsorption of the dye onto the fiber surface, and (4) diffusion of the dye into the fiber. The last step is widely considered to be the rate-determining step and is a popular topic of research [6–10].

However, according to previous studies, the dissolution rate of dye in supercritical carbon dioxide influences the overall dyeing time [11]. As the dissolution rate of the dye increases through the micronization of the dye particles, the overall dyeing time is shortened. The concentration of the solution is the driving force of the transfer of the dye from the supercritical solution to the fiber, which affects the dyeing time. When the dye dissolution rate is high, the dye uptake into a fiber is accelerated because the concentration of the supercritical solution can be maintained at a high value during the dyeing process. In general, dissolution rate is related to mass transfer coefficient and the reciprocal of

the overall mass transfer coefficient is expressed as the sum of the reciprocal of the mass transfer coefficients of the dispersed and continuous phases [12,13]. When the size of the dye particles decreases, the mass transfer coefficient of the dispersed phase increases, and the total mass transfer coefficient increases. Likewise, if the mass transfer coefficient of the continuous phase increases, the total mass transfer coefficient also increases, and the dyeing time can be expected to decrease.

The mass transfer coefficient of the continuous phase is related to the characteristic of flow of the fluid, which is affected by the flow rate, the structure of the pipe through which the fluid flows, and the shape of the internal structure. In the dyeing apparatus used in the supercritical dyeing process, the dye dissolution chamber is generally located in front of the dyeing cell where dyeing is performed and exhibits a cylindrical structure [2,14,15]. The diameter and length of the dye chamber affect the flow of fluid through it. In many studies, a change in the mass transfer coefficient of the continuous phase according to the length-to-diameter ratio (L/D ratio) was observed [16–18]. Therefore, changing the mass transfer coefficient by adjusting the geometry of the dye storage column can be a good option to improve the dissolution rate of the dye. Many researchers have described the relationship between fluid flow and mass transfer as a dimensionless correlation [17,19]. While dimensionless correlation itself describes the mass transfer of a system, it can also be used to predict mass transfer or fluid flow in other similar systems. Therefore, using this, it is possible to predict the results by applying the experimental results of a small lab-scale device to a larger device [20,21].

In general, kinetic studies of extraction or dissolution processes are conducted by observing the change in the mass or concentration of a substance over time. In this process, in situ UV/Vis spectrometry could be a suitable analysis method. The UV-Vis spectrophotometer is an accurate and universal device that measures the concentration of a solution. This device measures the concentration of a solution by calculating the absorbance at which a solute absorbs photons from the number of photons passing through the solution [22]. The advantage of using this device is that it can measure not only the concentration in the equilibrium state, but also the changes in concentration simultaneously. In addition, the in situ spectrometer can detect supercritical solutions without interference and detect low concentrations with high resolution. In fact, in many studies, an in situ UV/Vis spectrometer was used to analyze the dyeing process [22–27]. Using this analysis method, extraction or dissolution curves can be measured and obtained for a desired time without interruption.

The aim of this study is to investigate the effect of flow characteristics on the dissolution rate of dye in supercritical CO_2 and obtain conclusions that can be utilized to improve the efficiency of actual dyeing facilities. In this study, the differences in dissolution rate of dye for the continuous flow of supercritical carbon dioxide in dye columns at different L/D ratios and various experimental conditions were observed using in situ UV/Vis spectrometry. A dissolution kinetic model was designed and modified to calculate the mass transfer coefficient. Moreover, the relation between the flow of CO_2 and the mass transfer coefficient was investigated through an analysis of dimensionless correlation. Finally, using this correlation equation, the dissolution pattern in the scaled-up size column was predicted.

2. Materials and Methods

C.I. Disperse Red 60 (DR60) (99% purity) was supplied by Acroma Korea Corp. (Indong, Korea) without any additives or dispersants. The molecular structure of the disperse dye is shown in Figure 1. Carbon dioxide (CO_2) (99.5% purity) was purchased from Hyup-Sin Gas Co. (Seoul, Korea). All the materials were used without further purification.

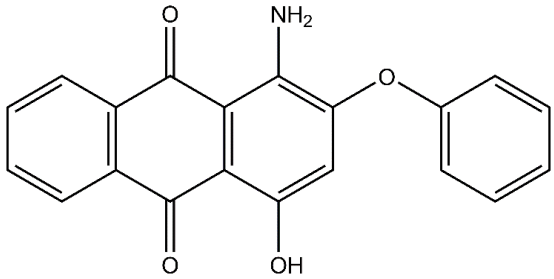

Figure 1. Chemical structure of DR60.

A schematic diagram of the dye-dissolving apparatus is shown in Figure 2. The apparatus was designed based on a study that analyzed diffusion behavior of disperse dye into a fiber using an extraction device [28]. To dissolve the dye under constant temperature and pressure conditions, a column (9) containing dye was installed in a high-pressure cell (8). The temperature of the cell was maintained while ethylene glycol was circulated as the heat medium using a circulation thermostat (3) (model: CW-05G, Lab Companion, Billerica, MA, USA) connected to a preheater (7). A 100-µm mesh filter was installed on both the inlet and outlet sides of the dye column to prevent the loss of undissolved dye without interfering with the flow of the fluid. In addition, the column was designed to be interchangeable. The outlet of the column was connected to the view cell (10) used to measure the concentration of the dye in CO_2 using an in situ UV/Vis spectrometer. On the view cell, two sapphire windows were installed to connect the UV-Vis spectrometer (11) (model: Avaspec-ULS2048CL-EVO, Avantes, The Netherlands) to the cell, along with a light source and detector. The distance between the two sapphire windows, the distance traveled by the light through the solution, was designed to be approximately 1.2 cm. The preheater, high-pressure cell, and view cell were placed inside an air bath (6) to precisely control the working temperature of the experiments. The detailed structure of the cylindrical dye column used in this study is shown in the Figure 3. In order to ignore the end effect at the inlet and outlet of the column, the diameter of the column inlet is designed to be the same as the inner diameter of the column. In addition, there is a space between the filter on the outlet side and the line that becomes smaller in diameter. The dye column was defined as the space between the two filters, and accordingly, the distance between the filters is the length of the dye column.

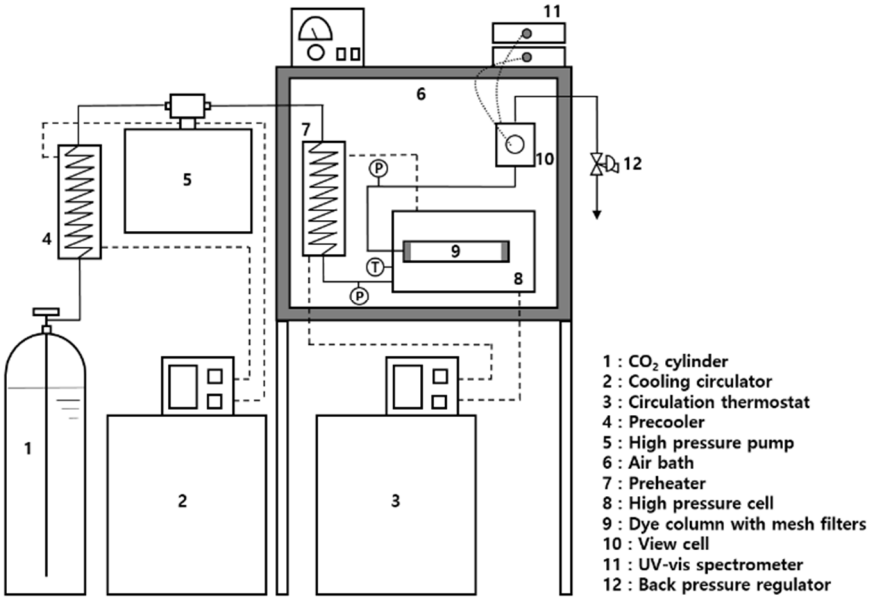

Figure 2. Schematic diagram of experimental apparatus.

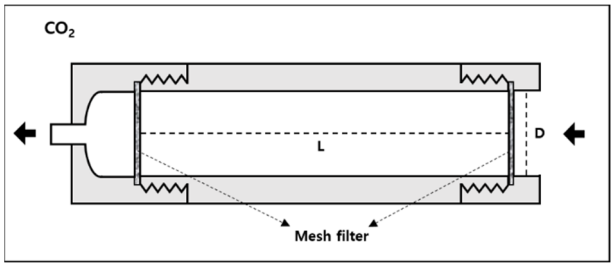

Figure 3. Structure of dye column.

The experimental sequence was as follows. First, the correct amount of dye was weighed and then loaded into the dye column. Filters were installed in the column, and the total weight of the column was measured. After the dye column was installed on the high-pressure cell, the cell was completely sealed. Subsequently, the assembled cell was placed in an air bath, the view cell and heating circulator were connected, and the temperature was raised. After the desired temperature was reached, the CO_2, chilled to −20 °C by a precooler (4) connected to a cooling circulator (2), was pumped using a dual-plunger high-pressure pump (5) (model: HKS-3000, Hanyang Accuracy, Hanyang, Korea). The pumped liquid CO_2 was heated to a supercritical state while passing through the preheater and injected into the cell. Simultaneously with the operation of the pump, the concentration of the passing CO_2 was analyzed by the in situ UV/Vis spectrometer through the measurement of the absorbance, which was recorded at every second and automatically stored on a computer. The experimental pressure was controlled at the desired conditions using a back pressure regulator (12) (model: 26-1700 series, Tescom, Pflugerville, TX, USA). The experiment was performed for 2 h under the conditions of 393.15 K and 25 MPa, which are general supercritical dyeing process conditions, and the time needed for pressurization was included. After the dye was dissolved for 2 h, the dye column was removed and weighed to obtain the amount of dissolved dye. In the experiment, the flow rates of CO_2 were 20, 30, and 40 mL/min. The experiment was conducted with columns exhibiting length-to-diameter ratios of 1, 5, and 10, and the volumes of all columns were almost identical. The sizes of the columns used in this study are shown in Table 1. The experiment was conducted three times under each experimental condition, and the average weight of the dissolved dye was used. The standard uncertainty of temperature, pressure, and gravimetric analysis is 0.1 MPa, 0.1 K, and 0.1 mg, respectively.

Table 1. Size of dye columns.

Length (m)	Diameter (m)	L/D Ratio	Volume (m^3)
0.0146	0.0146	1	2.44×10^{-6}
0.043	0.0086	5	2.45×10^{-6}
0.068	0.0068	10	2.45×10^{-6}

3. Results and Discussion

3.1. UV/Vis Spectrometer Analysis

To analyze the dissolution rate of the dye in supercritical CO_2, the concentration of the dye in supercritical CO_2 was measured using an in situ UV/Vis spectrometer. The Beer-Lambert law was used to calculate the concentration of the solution from the measured absorbance with two assumptions for application to the supercritical solution [23,27]. The first assumption is that the molar absorption coefficient is constant. In the supercritical state, the molar absorption coefficient is known to vary with density [24,29]. In this study, the dissolution of the dye was carried out under constant conditions of 393.15 K and 25 MPa; however, because the absorbance measurement included a pressurization step, the molar absorption coefficient was assumed to be constant, even as the pressure was increased. The second assumption is that the solute absorption is not affected by other solutes. This

assumption is generally justified when the solute concentration is low, and it is applicable because the solubility range of DR60 in supercritical CO_2 is 10^{-6} to 10^{-7} in terms of mole fraction. For this reason, many studies have shown that the absorbance and concentration have a linear relationship in supercritical solutions [30–32].

Absorbance is usually measured at a specific monochromatic wavelength, λ_{max}. In this study, because the fluid flows as the absorbance is measured, noise due to the flow can occur, and fluctuations occur near the top of the peak as a result of this noise. To minimize the error caused by this phenomenon, the absorbance was measured by specifying a range rather than a single wavelength. The absorbance spectrum of DR60 as a function of wavelength in supercritical CO_2 at 393.15 K and 25 MPa is shown in Figure 4. The maximum absorption peak appears at approximately 540 nm; however, the change in absorbance according to concentration of solution is large in that area. Therefore, in this experiment, absorbance was measured at a wavelength of 500–510 nm, and integrated absorbance was calculated with following equation.

$$A = \int_{\lambda_1}^{\lambda_2} \varepsilon(\lambda) d\lambda \cdot c \cdot l = \int_{\lambda_1}^{\lambda_2} \varepsilon \cdot c \cdot l d\lambda = \int_{\lambda_1}^{\lambda_2} A_\lambda d\lambda \quad (1)$$

where A is the integrated absorbance in the range of λ_1 and λ_2. $\varepsilon(\lambda)$ [L·mol^{-1}·cm^{-1}] is the molar absorption coefficient at λ, c [mol·L^{-1}] is the solute concentration in solution, and l [cm] is the path length of light. A_λ is monochromatic absorbance at wavelength λ. Using above assumption, $\varepsilon(\lambda)$ is constant at experimental condition in this study. In all subsequent calculations, the integrated value was used for absorbance.

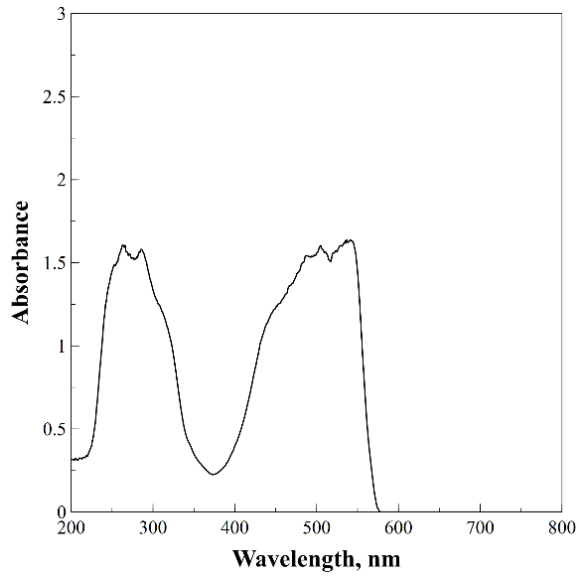

Figure 4. Absorbance spectrum of DR60 in CO_2 at 393.15 K, 25 MPa.

3.2. Calculation of Mass Transfer Coefficient

The change in the integrated absorbance over time in the wavelength range of 500–510 nm is shown in Figure 5. This figure shows the case where approximately 40 mg of dye was put into a dye column with an L/D ratio of 10 and the experiment was conducted under the condition of a CO_2 flow rate of 30 mL/min. By calculating the area of the graph of the change in absorbance over time, the accumulated absorbance for that time can be obtained. According to the Beer-Lambert law, absorbance and dye concentration have a linear relationship. That is, the accumulated absorbance and concentration of dissolved dye are proportional to each other. To convert the measured absorbance into the amount of dye, the volume of the solution passing through the view cell is assumed to be always constant. Using this assumption, since the concentration of the dye is proportional to the

weight of the dye, it can be said that the cumulative absorbance over 2 h (120 min) has a linear relationship with the weight of the dissolved dye.

$$A_{accumulated,t} = \int_0^t A dt \tag{2}$$

$$A_{accumulated,120} : m_{120} = A_{accumulated,t} : m_t \tag{3}$$

$$m_t = \frac{m_{120} \times A_{accumulated,t}}{A_{accumulated,120}} \tag{4}$$

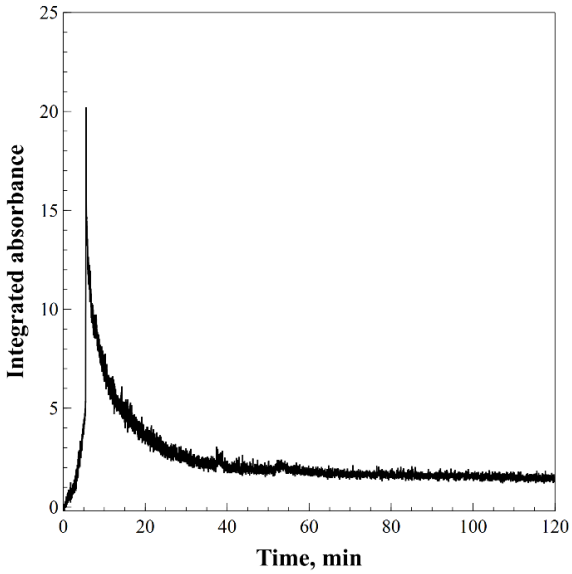

Figure 5. Time-dependent absorbance changes for DR60, column with L/D ratio = 10 and flow rate = 30 mL/min.

$A_{accumulated,t}$ and m_t [mg] are the cumulative absorbance at time t [min] and total amount of the weight of the dye dissolved and exiting the dye column, respectively. Using Equation (4), the absorbance over time measured in each experiment was converted into the total amount of dye dissolved over time to obtain a dye dissolution curve. Figure 6 shows a graph of the cumulative amount of dye dissolved over time for the addition of approximately 40 mg of dye at a flow rate of 30 mL/min and a dye column with an L/D ratio of 10. The experimental conditions and measurement results are shown in Table 2. When comparing the amount of dye dissolved under each experimental condition, a greater L/D ratio and flow rate correspond to an improved dissolution efficiency over 2 h.

Table 2. Experimental conditions and measured value.

Flow Rate [mL/min]	L/D Ratio	Initial Dye [1] [mg]	Dissolved Dye [2] [mg]
20	1	39.8	6.73 (0.65)
	5	41.0	15.31 (0.52)
	10	40.6	19.59 (2.01)
30	1	39.3	7.60 (0.22)
	5	40.3	17.02 (0.71)
	10	40.9	22.68 (1.10)
40	1	40.1	8.80 (0.44)
	5	40.3	18.11 (1.02)
	10	41.2	28.93 (0.51)

[1] Uncertainty for the measured values: u (initial dye) = 0.1. [2] Averaged values and the standard deviation (in the parentheses) for the data having three measurements at each condition.

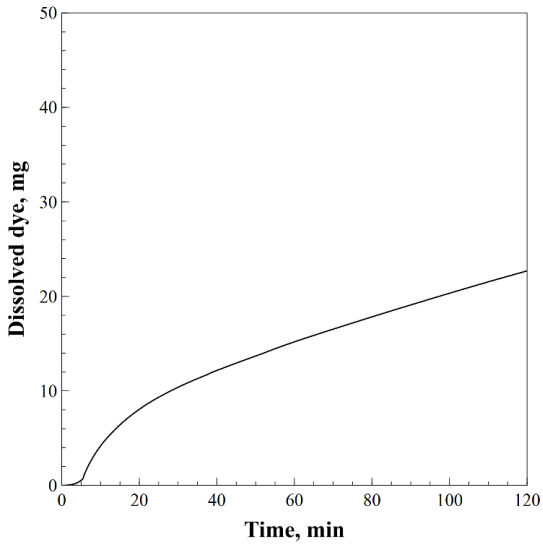

Figure 6. Weight of dissolved dye as a function of time, column with L/D ratio = 10 and flow rate = 30 mL/min.

A simplified dissolution model was designed to calculate the mass transfer coefficient of the system constructed in this experiment, based on the amount of dissolved dye.

$$\frac{dM}{dt} = -K_c A(t)(C_s - C_b) \tag{5}$$

where M is the weight of the dye in the dye column, K_c [m·min^{-1}] is the mass transfer coefficient, $A(t)$ [m^2] is the total surface area of the dye at time t, and C_s and C_b are the saturation concentration and bulk concentration of the dye in the fluid. Equation (5) represents the basic dissolution rate equation [12,13]. In this study, this equation was improved through two assumptions, for applying the above equation to the system. First, because fresh CO_2 is continuously supplied, the concentration of the bulk fluid is assumed to be zero. Second, each dye particle was assumed to participate in the dissolution, with all the dye particles being spherical. The surface area of the dye can be calculated as follows,

$$A_{dye} = 4\pi {r_{dye}}^2 \tag{6}$$

$$N_{dye,t} = \frac{M_t}{Average\ mass\ of\ dye\ particles} = \frac{M_t}{\rho V_{dye}} \tag{7}$$

$$V_{dye} = \frac{4}{3}\pi {r_{dye}}^3 \tag{8}$$

$$A(t) = A_{dye} \times N_{dye,t} = A_{dye} \times \frac{M_t}{\rho V_{dye}} \tag{9}$$

where A_{dye} [m^2], r_{dye} [m], and V_{dye} [m^3] are the average surface area, particle radius, and particle volume of DR60, respectively. M_t [g] is the mass of the dye in the column at time t [min]. ρ is the density of DR60 calculated with molecular weight and molar volume, which is provided by supplier. In this study, r_{dye} was calculated as 20 µm, which was measured in the previous study [11]. From Equation (9), the surface area of the dye can be expressed as a function of the mass of the dye,

$$\frac{dM}{dt} = -kM_t \tag{10}$$

$$k = \frac{3K_c C_s}{\rho r_{dye}} \tag{11}$$

Substituting Equation (9) into Equation (5) and substituting k for constant values give Equation (10).

$$\frac{M_t}{M_0} = e^{-kt} \tag{12}$$

Integrating Equation (10) yields Equation (12), and the mass transfer coefficient can be calculated from the change in the mass of the dye in the column over time. The change in the mass of dye for each experimental condition is presented in Figure 7. M_t is calculated by subtracting the value previously calculated from the absorbance from M_0. To reduce the error of the absorbance noise, points were plotted every 10 min, with the trend line for each condition indicated by a dotted line. For the trend line equation, the curve fitting program from MATLAB was used. As shown in the graph, each trend line is not fitted well in the front part. In this experiment, the total experiment time includes the pressurization time; thus, the fluid does not flow well, and the dye can remain in contact for a sufficient time such that the dye is dissolved at the beginning. Therefore, it was found that more dyes were dissolved in the beginning than what the trend line indicated. For this reason, 20 min was set as the initial value for a better fitting. It was assumed that the time required for the pressure to reach the desired value and almost all of the carbon dioxide dissolving a large amount of dye initially escaped was 20 min. The time taken for the pressure to increase was about 10 min when the flow rate was 20 mL/min and about 6 min when the flow rate was 30 mL/min. Therefore, values from 20 min were used so that the dissolution phenomenon was observed only when pure CO_2 flows in the experiment. The modified graph is shown in Figure 8. The equation for each trend line is shown in Table 3. From the equation of the trend line, the experimental fitting constant k can be obtained, and the mass transfer coefficient (K_c) can be calculated using Equation (11) above. The mass transfer coefficients of each experimental conditions are listed in Table 3. The density of DR60, which is required to calculate the mass transfer coefficient, is obtained from the dye supplier, and the solubility of DR60 at 393.15 K and 25 MPa was 1.1343×10^{-4} g/mL, which was experimentally measured using static method with UV/Vis spectrometer. The values used in the calculation of mass transfer coefficient are listed in Table 4. This calculation revealed that the larger the L/D ratio and the higher the flow rate conditions were, the greater the mass transfer coefficient was. Furthermore, when the L/D was small, the difference in dissolution rate according to the flow rate was not large, and as the L/D increased, the difference in dissolution rate according to the flow rate increased.

Table 3. Equation of trend lines.

Flow Rate [mL/min]	L/D Ratio	Trend Line Equation	R^2	$K_c \cdot 10^4$ [m/min] [1]
20	1	$y = e^{-0.00130x}$	0.9908	1.093
	5	$y = e^{-0.00346x}$	0.9927	2.927
	10	$y = e^{-0.00536x}$	0.9941	4.533
30	1	$y = e^{-0.00132x}$	0.9685	1.120
	5	$y = e^{-0.00372x}$	0.9488	3.144
	10	$y = e^{-0.00592x}$	0.9981	5.007
40	1	$y = e^{-0.00160x}$	0.9883	1.352
	5	$y = e^{-0.00413x}$	0.9938	3.497
	10	$y = e^{-0.00734x}$	0.9989	6.215

[1] Calculated with Equation (11).

Table 4. Values used in the calculation of mass transfer coefficient.

Property of DR60	Value
Density of DR60 [g/mL]	1.44
Particle radius of DR60 [μm]	20
Solubility of DR60 in CO_2 [g/mL]	1.134×10^{-4}

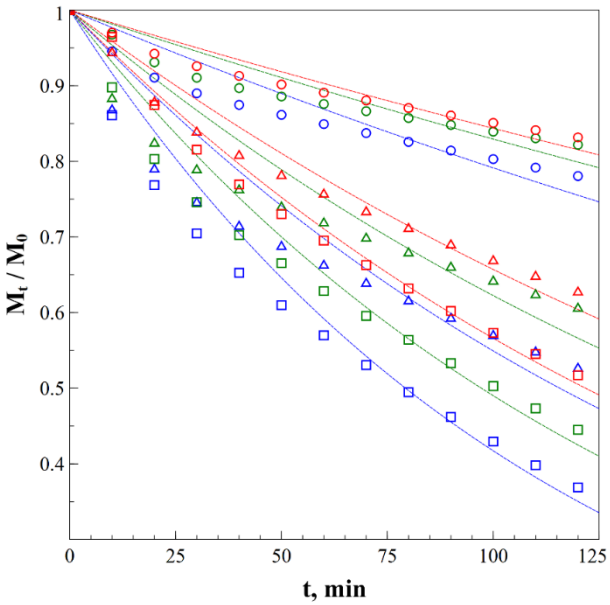

Figure 7. Dimensionless concentration as function of time for various experimental conditions and trend lines with flow rate = 20 mL/min (red), flow rate = 30 mL/min (green), flow rate = 40 mL/min (blue), L/D = 1 (○), L/D = 5 (△), L/D = 10 (□).

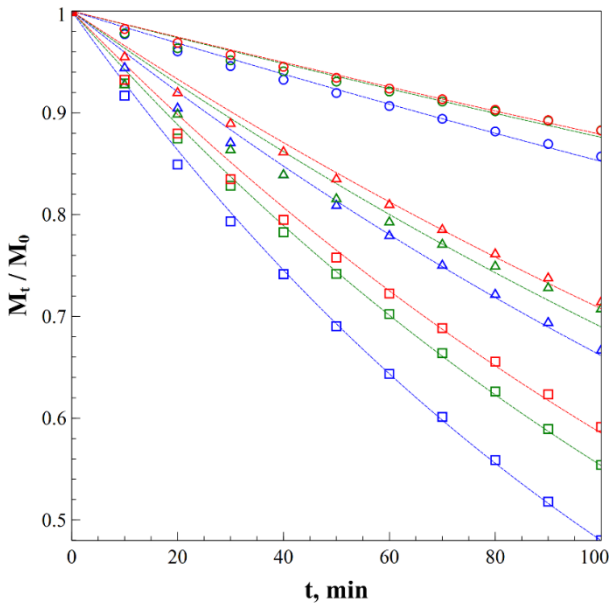

Figure 8. Modified dimensionless concentration as a function of time for various experimental conditions and trend lines with flow rate = 20 mL/min (red), flow rate = 30 mL/min (green), flow rate = 40 mL/min (blue), L/D = 1 (○), L/D = 5 (△), L/D = 10 (□).

3.3. Effect of Initial Weight of Dye

To check the effect of the initial mass of the dye entering the column on the dissolution rate, the experiment was performed with different initial masses at a flow rate of 30 mL/min in a column with an L/D ratio of 10. As above, the amount of dye at 20 min was set as an initial value and the trend line and mass transfer coefficient were calculated. The weight changes of the dyes in the column over time and the trend line are shown in Figure 9, and the experimental conditions and results are shown in Table 5. Data fitting was performed to determine the relationship between the initial mass of the dye and the mass transfer

coefficient, which was found to be almost linear. The results are shown in Figure 10. The fitting equation is

$$K_c = -6 \cdot 10^{-6} M_0 + 0.0007,\ R^2 = 0.9999, \quad (13)$$

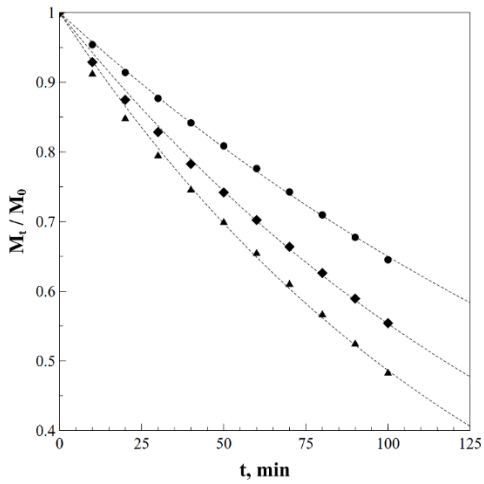

Figure 9. Dimensionless concentration as a function of time and trend lines, column with L/D ratio = 10 and flow rate = 30 mL/min for various initial weight of dye, 62.4 mg (●), 40.9 mg (♦), 20.2 mg (▲).

Table 5. Experimental conditions and results: Effect of initial weight.

Initial Dye [mg]	M_0 [1] [mg]	Dissolved Dye [2] [mg]	Trend Line Equation	R^2	K_c 10^4 [m/min]
20.2	14.51	13.21 (1.58)	$y = e^{-0.00721x}$	0.9974	6.10
40.9	32.84	22.68 (1.10)	$y = e^{-0.00592x}$	0.9981	5.01
62.4	55.02	26.90 (2.71)	$y = e^{-0.00431x}$	0.9993	3.65

[1] Calculated value from Absorbance of DR60. [2] Averaged values and the standard deviation (in the parentheses) for the data with three measurements at each condition.

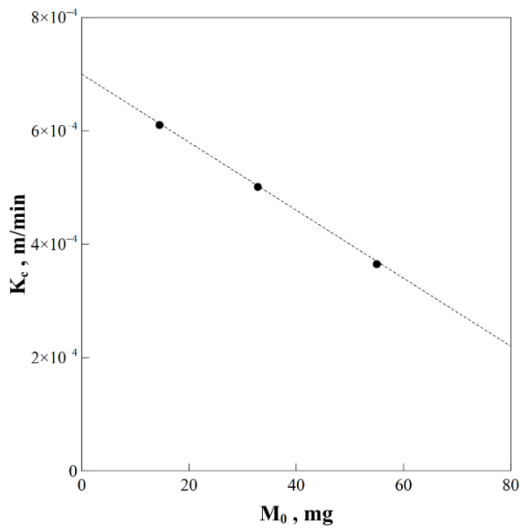

Figure 10. Initial weight of dye dependent on the mass transfer coefficient of DR60 and fitting line.

According to the results, an increase in the initial mass of the dye corresponds to a decrease in the dissolution mass transfer coefficient of the dye. In general, the melting point of DR60 is known to be 185 °C. However, according to the study results that melting-point depression may occur in a high-pressure CO_2 environment, dye particles can be aggregated even under this experimental condition [33]. This is interpreted as the increase in the initial

mass of the dye causes the aggregation of the dye particles to increase, which gradually reduces the surface area of the particles that can participate in dissolution. In the dissolution rate model used to calculate the mass transfer coefficient, it was assumed that all particles were in contact with carbon dioxide, but in reality, there were some particles that did not make contact with carbon dioxide. As the dye particles overlap due to agglomeration or aggregation, etc., an area in which carbon dioxide cannot directly contact occurs, and this phenomenon can increase in proportion to the amount of dye. As a result, as the amount of dye increases, the mass transfer coefficient is calculated to be small. According to this result, when calculating the mass transfer coefficient, the equation must be corrected in consideration of the effective surface area. This is because, according to dimensionless correlation, in the case of theoretically the same *Re*, K_c should be equal regardless of M_0. In this study, the modified mass transfer coefficient (K_c*) was calculated as follows by applying Equation (13) to K_c calculated from Equation (11).

$$K_c^* = K_c + 6 \cdot 10^{-6} M_0 \tag{14}$$

3.4. Dimensionless Correlation

In this study, the change in the dye dissolution rate according to the L/D ratio of the dye column was observed. When other experimental conditions such as CO_2 flow rate, volume of dye column, weight of dye, temperature, and pressure are constant, the L/D ratio affects the flow of CO_2. When the diameter of the column is changed, the cross-sectional area of the space through which the fluid flows changes. Then, when the volumetric flow rate of the fluid remains the same, the velocity of the fluid changes. The characteristics of flow according to these structural variables and flow rate are expressed as the Reynolds number (*Re*). In the case of convective mass transfer, the relationship between the fluid flow and the properties of fluid and materials is generally expressed as the following correlation [13,19],

$$\mathrm{Sh} = f(Re,\ Sc) = aRe^m Sc^n \tag{15}$$

where Sh is the Sherwood number, *Re* is the Reynolds number, *Sc* is the Schmidt number, and *a*, *m*, and *n* are constants. Sh, *Re*, and *Sc* are defined by Equations (16)–(18), respectively,

$$\mathrm{Sh} = \frac{K_c L}{D_{AB}} \tag{16}$$

$$\mathrm{Re} = \frac{\rho U L}{\mu} \tag{17}$$

$$\mathrm{Sc} = \frac{\mu}{\rho D_{AB}} \tag{18}$$

where L [m] is the characteristic length, D_{AB} is the diffusivity of dye in supercritical CO_2, ρ is the density of CO_2, U is the velocity of CO_2, and μ is the viscosity of CO_2. In the system of this study, the characteristic length was a diameter of dye. The density and viscosity of CO_2 were obtained from the National Institute of Standards and Technology (NIST, USA) Chemistry webbook [34]. The diffusion coefficient in the supercritical CO_2 of DR60 was calculated as 6×10^{-7} m^2/min by referring to the values of other dyes that are judged to have similar scale values with DR60, as there are no measured values or values in the literature about diffusivity of DR60 [35]. The values used to calculate the dimensionless number are shown in Table 6. The calculated dimensionless numbers and their correlation equations are listed in Table 7. *Sc* is a value that does not change for each experiment under this experimental condition, because both the diffusion coefficient, density, and viscosity are functions of temperature and pressure. Therefore, the correlation was calculated only with Sh and *Re* and not with *Sc*. The dimensionless numbers for each condition are shown in Figure 11, with the fitting parameters calculated using the MATLAB curve fitting program.

Table 6. Values used in the calculation of dimensionless numbers.

Property	Value
Density of CO_2 [Kg/m^3]	500
Viscosity of CO_2 [Kg/m· s]	4×10^{-5}
Particle radius of DR60 [μm]	20
Diffusivity of DR60 in CO_2 [m^2/min]	6×10^{-7}

Table 7. Calculated dimensionless numbers and correlation equations.

Flow Rate [mL/min]	L/D Ratio	K_c*·10^4 [1] [m/min]	*Re*	Sh	Dimensionless Correlation	R^2
20	1	3.344	0.996	0.0222	$Sh = 0.0221 \cdot Re^{0.442}$	0.9912
	5	5.087	2.869	0.0339		
	10	6.664	4.589	0.0444		
30	1	3.316	1.493	0.0221	$Sh = 0.0180 \cdot Re^{0.477}$	0.9911
	5	5.214	4.304	0.0348		
	10	6.978	6.884	0.0465		
40	1	3.544	1.991	0.0236	$Sh = 0.0161 \cdot Re^{0.514}$	0.9624
	5	5.432	5.738	0.0362		
	10	8.052	9.178	0.0537		

[1] Modified with Equation (14).

According to dimensionless correlation equations, in the dissolution model of the dye used in this study, Sh is proportional to the 0.442–0.514 power of *Re*. In general, in the case of extraction using supercritical fluid in a packed bed system, the dimensionless correlation shows that the index of *Re* is approximately 0.5–0.83 [19]. In this study, empty spaces exist inside the column because the column is not fully packed full of dye particles. Therefore, it is interpreted that the influence of the flow properties of the fluid itself on the dissolution of the dye is reduced. In addition, the tendency varies depending on the flow rate. This is because in this study, when the flow rate was changed, the volume was constant, so there was a difference in the time the fluid stayed in the column.

3.5. Prediction of Dissolution Rate

A dye dissolution experiment was conducted with a large volume dye column to test whether the result obtained above can be applied to a larger size dyeing equipment. In order to make the space time (the time that the carbon dioxide stays in the column) equal to the case where the flow rate is 30 mL/min in a column with a small volume, the flow rate was performed at 77 mL/min. Furthermore, about 100 mg of dye was inserted to match the ratio of the total amount of CO_2 and dye. The Sherwood number was calculated under the experimental conditions using the dimensionless correlation equation at the previously calculated flow rate of 30 mL/min. From this, the dissolution rate constant (k) was calculated to predict the dissolution curve. The values used in the calculation are shown in Table 8. In addition, Figure 12 shows the experimentally measured dissolution curve and the calculated dissolution curve. As a result of predicting the dissolution rate using the dissolution rate model derived in this study, it was almost accurately predicted with an error of about 2.4%. Actually, when applied to industrial dyeing facilities, differences may occur due to various additional process variables, but it was confirmed that the possibility of empirically predicting the rate of dye dissolution when increasing the volume of the dye column.

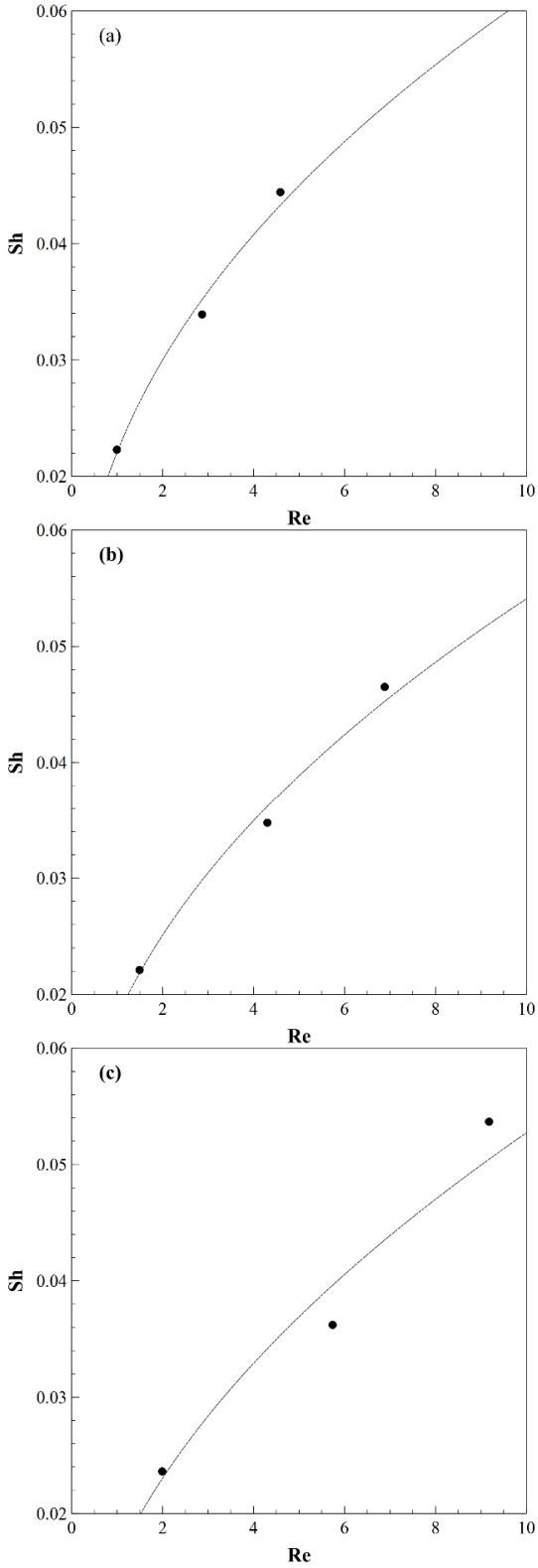

Figure 11. Dimensionless correlation, flow rate = 20 mL/min (**a**), flow rate = 30 mL/min (**b**), flow rate = 40 mL/min (**c**).

Table 8. Values used in the calculation for prediction of dissolution curve.

Property	Value
Length of dye column [m]	0.093
Diameter of dye column [m]	0.0093
Volume of dye column [m^3]	6.32×10^{-6}
Flow rate of CO_2 [ml/min]	77
Initial dye [mg]	100.7
Dissolved dye [mg]	39.4
Re	9.446
Experimented dissolution curve	$y = e^{-0.00332x}$
Predicted dissolution curve	$y = e^{-0.00324x}$

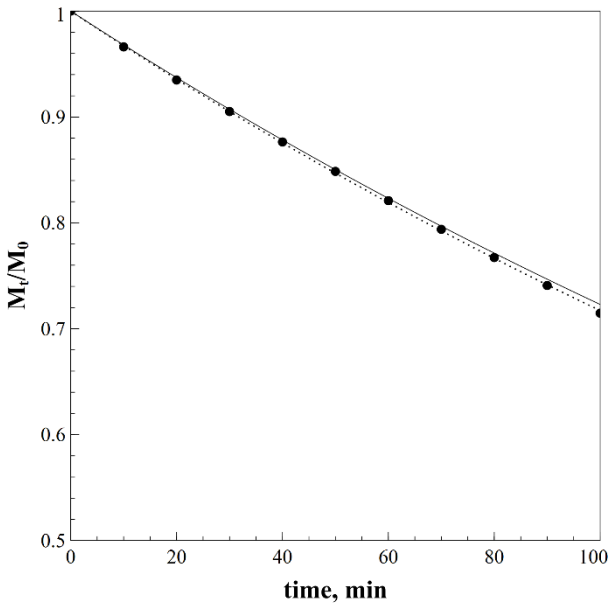

Figure 12. Dissolution curve with large size dye column, experimented line (dotted) and predicted line (solid).

4. Conclusions

In a system in which supercritical CO_2 flows continuously, the dissolution rate of DR60 was experimentally measured, and a dissolution kinetic model was designed to calculate the mass transfer coefficient for dye to CO_2 phase. A method for measuring and expressing the dissolution rate of dyes with in situ UV/Vis spectrometer were demonstrated. The dissolution rate of the dye was calculated by converting the absorbance to the mass of the dye based on the Beer-Lambert law. The mass transfer coefficient of DR60 in the continuous supercritical system could be obtained from experimental results. By changing the L/D ratio of the dye column in which the dye and supercritical CO_2 are in contact with each other, the dissolution rate of the dye was found to increase as the flow velocity increased. The relationship between the mass transfer coefficient and the fluid flow was expressed through the correlation between Sh and *Re*. Finally, using this correlation equation, the dissolution rate at which the dye dissolves in the scale-up dye column was accurately predicted with an error of about 2.4%. The system established in this study simulated the actual dyeing process similarly, and the results explain this system well. Therefore, this system can help to make the process more efficient and contribute to broadening the understanding of reactor and process design in the supercritical dyeing process. In addition, this study is expected to be able to be applied to predict the end point of the process.

Author Contributions: Conceptualization, G.P.; data curation, G.P., D.E.K., and W.K.; formal analysis, G.P.; investigation, G.P., D.E.K., and W.K.; methodology, G.P.; software, G.P.; supervision, Y.-W.L.; validation, J.P.; writing—original draft, G.P.; writing—review and editing, Y.-W.L. All authors have read and agreed to the published version of the manuscript.

Funding: This work was supported by the Nurture Project of Water-Less Color Industry (10078329, Development of 200 kg—class dyeing facility and process using supercritical fluid), funded by the Ministry of Trade, Industry and Energy (MOTIE) of Korea.

Institutional Review Board Statement: Not applicable.

Informed Consent Statement: Not applicable.

Acknowledgments: The Institute of Engineering Research at Seoul National University provided research facilities for this work.

Conflicts of Interest: The authors declare that there is no conflict of interest.

References

1. Banchero, M. Supercritical fluid dyeing of synthetic and natural textiles—A review. *Color. Technol.* **2013**, *129*, 2–17. [CrossRef]
2. Kim, T.; Park, G.; Kong, W.; Lee, Y.-W. Supercritical Dyeing Technology. *Clean Technol.* **2018**, *24*, 1–8. [CrossRef]
3. Abou Elmaaty, T.; Sofan, M.; Elsisi, H.; Kosbar, T.; Negm, E.; Hirogaki, K.; Tabata, I.; Hori, T. Optimization of an eco-friendly dyeing process in both laboratory scale and pilot scale supercritical carbon dioxide unit for polypropylene fabrics with special new disperse dyes. *J. CO2 Util.* **2019**, *33*, 365–371. [CrossRef]
4. Bai, T.; Kobayashi, K.; Tamura, K.; Jun, Y.; Zheng, L. Supercritical CO_2 dyeing for nylon, acrylic, polyester, and casein buttons and their optimum dyeing conditions by design of experiments. *J. CO2 Util.* **2019**, *33*, 253–261. [CrossRef]
5. Wang, Y.; Jing, X.; Zhao, Y.; Zheng, L.; Zheng, H. Waterless beam dyeing in supercritical CO_2: Establishment of a clean and efficient color matching system. *J. CO2 Util.* **2021**, *43*, 101368. [CrossRef]
6. Özcan, A.S.; Özcan, A. Adsorption behavior of a disperse dye on polyester in supercritical carbon dioxide. *J. Supercrit. Fluids* **2005**, *35*, 133–139. [CrossRef]
7. Sicardi, S.; Manna, L.; Banchero, M. Comparison of dye diffusion in poly(ethylene terephthalate) films in the presence of a supercritical or aqueous solvent. *Ind. Eng. Chem. Res.* **2000**, *39*, 4707–4713. [CrossRef]
8. Sicardi, S.; Manna, L.; Banchero, M. Diffusion of disperse dyes in PET films during impregnation with a supercritical fluid. *J. Supercrit. Fluids* **2000**, *17*, 187–194. [CrossRef]
9. Fernandez Cid, M.V.; Van Der Kraan, M.; Veugelers, W.J.T.; Woerlee, G.F.; Witkamp, G.J. Kinetics study of a dichlorotriazine reactive dye in supercritical carbon dioxide. *J. Supercrit. Fluids* **2004**, *32*, 147–152. [CrossRef]
10. Bach, E.; Cleve, E.; Schollmeyer, E. Past, present and future of supercritical fluid dyeing technology—An overview. *Rev. Prog. Color. Relat. Top.* **2002**, *32*, 88–102. [CrossRef]
11. Kim, T.; Seo, B.; Park, G.; Lee, Y.-W. Effects of dye particle size and dissolution rate on the overall dye uptake in supercritical dyeing process. *J. Supercrit. Fluids* **2019**, *151*, 1–7. [CrossRef]
12. Seager, R.J.; Acevedo, A.J.; Spill, F. Solid dissolution in a fluid solvent is characterized by the interplay of surface area-dependent diffusion and physical fragmentation. *Sci. Rep.* **2018**, 1–17. [CrossRef]
13. Welty, J.R.; Wicks, C.E.; Wilson, R.E.; Rorrer, G. *Fundamentals Of Momentum, Heat, And Mass Transfer*, 5th ed.; Wiley India: New Delhi, India, 2010; ISBN 8126528389.
14. Banchero, M.; Sicardi, S.; Ferri, A.; Manna, L. Supercritical Dyeing of Textiles—From the Laboratory Apparatus to the Pilot Plant. *Text. Res. J.* **2008**, *78*, 217–223. [CrossRef]
15. Banchero, M. Recent advances in supercritical fluid dyeing. *Color. Technol.* **2020**, *136*, 317–335. [CrossRef]
16. Duba, K.S.; Fiori, L. Supercritical CO_2 extraction of grape seed oil: Effect of process parameters on the extraction kinetics. *J. Supercrit. Fluids* **2015**, *98*, 33–43. [CrossRef]
17. Pérez-Galindo, J.A.; López-Miranda, J.; Martín-Dominguez, I.R. Geometric and Reynolds number effects on oregano (Lippia Berlandieri Schauer) essential oil extraction. *J. Food Eng.* **2000**, *44*, 127–133. [CrossRef]
18. Núñez, G.A.; Del Valle, J.M. Supercritical CO_2 oilseed extraction in multi-vessel plants. 2. Effect of number and geometry of extractors on production cost. *J. Supercrit. Fluids* **2014**, *92*, 324–334. [CrossRef]
19. Lin, T.M.; Ping, T.S.; Saptoro, A.; Freddie, P. Mass Transfer Coefficients and Correlation of Supercritical Carbon Dioxide Extraction of Sarawak Black Pepper. *Int. J. Food Eng.* **2013**. [CrossRef]
20. Thirteen, C. Scale-Up in Reactor Design. In *Modeling of Chemical Kinetics and Reactor Design*; Elsevier: Amsterdam, The Netherlands, 2001; pp. 1034–1081.
21. Donati, G.; Paludetto, R. Scale up of chemical reactors. *Catal. Today* **1997**, *34*. [CrossRef]
22. Braeuer, A. *In Situ Spectroscopic Techniques at High Pressure*; Elsevier: Amsterdam, The Netherlands, 2015; ISBN 9780444634221.
23. Ngo, T.T.; Bush, D.; Eckert, C.A.; Liotta, C.L. Spectroscopic measurement of solid solubility in supercritical fluids. *AIChE J.* **2001**, *47*, 2566–2572. [CrossRef]

24. Inomata, H.; Yagi, Y.; Saito, M.; Saito, S. Density dependence of the molar absorption coefficient—Application of the beer-lambert law to supercritical CO_2—Naphthalene mixture. *J. Supercrit. Fluids* **1993**, *6*, 237–240. [CrossRef]
25. Ngo, T.T.; Liotta, C.L.; Eckert, C.A.; Kazarian, S.G. Supercritical fluid impregnation of different azo-dyes into polymer: In situ UV/Vis spectroscopic study. *J. Supercrit. Fluids* **2003**, *27*, 215–221. [CrossRef]
26. Kautz, C.B.; Schneider, G.M.; Shim, J.J.; Wagner, B.; Tuma, D. Solubilities of a 1,4-bis(alkylamino)-9,10-anthraquinone series in compressed carbon dioxide. *J. Chem. Eng. Data* **2008**, *53*, 2356–2371. [CrossRef]
27. Wagner, B.; Nishioka, M.; Tuma, D.; Maiwald, M.; Schneider, G.M. Sample purification for spectroscopic high-pressure investigations by dynamic supercritical fluid extraction. *J. Supercrit. Fluids* **1999**, *16*, 157–165. [CrossRef]
28. Kim, T.; Seo, B.; Park, G.; Lee, Y.-W. Predicting diffusion behavior of disperse dyes in polyester fibers by a method based on extraction. *J. Supercrit. Fluids* **2020**, *157*, 104685. [CrossRef]
29. Rice, J.K.; Niemeyer, E.D.; Bright, F.V. Evidence for Density-Dependent Changes in Solute Molar Absorptivities in Supercritical CO_2: Impact on Solubility Determination Practices. *Anal. Chem.* **1995**, *67*, 4354–4357. [CrossRef]
30. Carrott, M.J.; Wai, C.M. UV—Visible Spectroscopic Measurement of Solubilities in Supercritical CO_2 Using High-Pressure Fiber-Optic Cells. *Anal. Chem.* **1998**, *70*, 2421–2425. [CrossRef]
31. Haarhaus, U.; Swidersky, P.; Schneider, G.M. High-pressure investigations on the solubility of dispersion dyestuffs in supercritical gases by VIS/NIR-spectroscopy. Part I—1,4-Bis-(octadecylamino)-9,10-anthraquinone and disperse orange in CO_2 and N_2O Up to 180 MPa. *J. Supercrit. Fluids* **1995**, *8*, 100–106. [CrossRef]
32. Suzuki, S.; Aoki, K.; Moribe, K.; Sako, T. Solubility Measurement in Supercritical CO_2 with High Pressure UV/VIS Absorption Spectroscopy. In *Asian Pacific Confederation of Chemical Engineering Congress Program and Abstract*; The Society of Chemical Engineers: Tokyo, Japan, 2004; p. 839. [CrossRef]
33. Yoon, T.J.; Youn, Y.S.; Son, W.S.; Seo, B.; Ahn, K.H.; Lee, Y.-W. Dimensionless entropy of fusion as a simple criterion to predict agglomeration in the supercritical antisolvent process. *Cryst. Growth Des.* **2013**, *13*, 3481–3489. [CrossRef]
34. Lemmon, E.; McLinden, M.O.; Friend, D.G. Thermophysical Properties of Fluid Systems. In *NIST Chemistry WebBook*; Linstrom, P.J., Mallard, W.G., Eds.; NIST Standard Reference Database Number 69; National Institute of Standards and Technology: Gaithersburg, MD, USA, 2018. [CrossRef]
35. Funazukuri, T.; Yamasaki, T.; Taguchi, M.; Yi, C. Fluid Phase Equilibria Measurement of binary diffusion coef fi cient and solubility estimation for dyes in supercritical carbon dioxide by CIR method. *Fluid Phase Equilib.* **2016**, *420*, 7–13. [CrossRef]